Solid-State Electronics 53 (2009) 1273–1279

Contents lists available at ScienceDirect

Solid-State Electronics

journal homepage: www.elsevier.com/locate/sse

Comparisons between intrinsic bonding defects in d^0 transition metal oxide such as HfO_2, and impurity atom defects in d^0 complex oxides such as $GdScO_3$

Gerald Lucovsky [a,*], Kwun-Bum Chung [d], Leonardi Miotti [a], Karen Pas Bastos [a], Carolina Amado [b], Darrell Schlom [b,c]

[a] North Carolina State University, Department of Physics, Raleigh, NC 27695-8202, USA
[b] Penn State University, Department of Materials Science and Engineering, State College, PA 16802-5005, USA
[c] Cornell University, Department of Materials Science and Engineering, Ithaca, NY 14853-1501, USA
[d] Dankook University, Department of Physics, Dongnamgu Anseodong 29, Cheonan 330-714, Republic of Korea

ARTICLE INFO

Article history:
Received 26 May 2009
Received in revised form 19 August 2009
Accepted 19 October 2009

The review of this paper was arranged by Dr. M.C. Lemme

Keywords:
Transition metal elemental oxides
Complex oxides
Vacancy defects
Alternative valence defects and alloy atoms
Insulator metal phase transition

ABSTRACT

This article addresses O-atom vacancy defects in the d^0 transition metal (TM) oxides HfO_2 and TiO_2, and Ti substitutions for Sc in the d^0 complex oxide $GdScO_3$. In each instance this results in occupied TM atoms with d^1 state representations. These are important for different aspects of the ultimate scaling limits for performance and functionality in nano-scale Si devices. The occupancy of d^1 states is cast in terms of many-electron theory in order to determine the effects of correlation on device performance and functionality. The first section of this article identifies equivalent d-state representations using on an ionic model for the effective valence states of Ti and Hf atoms bordering on O-atom vacancy defects. Removal of an O atom to create a neutral vacancy; this is equivalent to the bonding of two electrons to each vacancy site. This give rise to two coupled d^1 states for a mono-vacancy defect. Transitions from these occupied states generate spectroscopic features in the (i) pre-edge shake-up, and (ii) virtual bound state (VBS) shake-off energy regimes in O K edge XAS spectra. The number of states confirm that these are mono-vacancy defects. The second section addresses incorporation of Ti tetravalent impurities into trivalent $GdScO_3$, forcing Ti into a Ti^{3+} state and generating a d^1 electronic structure. Vacancy defect concentrations in HfO_2 are generally $<10^{19}\,cm^{-3}$. However, the Ti solubility in $GdScO_3$ is higher, and relative concentrations in excess of 16–17% lead to an insulator to metal transition with a ferri-magnetic electronic structure.

1. Introduction

It is well established that the ultimate limits of Si device scaling with increased performance and functionality require the replacement of SiO_2 and Si oxynitride alloy gate dielectrics with transition metal oxides and silicates with higher dielectric constants in order to continue Moore's law scaling into the nano-scale regime of lateral device dimensions [1]. Higher dielectric constants allow the use of physically thicker films for the required levels of dielectric capacitance while at the same time maintaining tunneling leakage currents that do not degrade device performance. In addition, there has been a need to increase chip functionality, e.g., by introducing ferro-magnetic and ferroelectric thin film layers [2], and in particular multiferroic materials in which there are opportunities for novel device configurations with coupled magnetic and ferroelectric functionality [3]. These ferro-magnetic, ferroelectric and muliferroic films are generally complex oxides comprised of first row transition metals, and either lanthanide rare earth or normal metal atoms. Both the intrinsic bonding defect states, as well as the magnetic and ferroelectric functionality generally involve occupied d-states, and/or occupied f-states, and as such increased attention must be given to the integration of a many-electron theory and experiment in evaluating thin film materials for device applications on the one hand [2,4], and explaining device properties and limitations imposed by intrinsic bulk and interface defects as well.

The requires the development of a new paradigm that takes into account differences between this challenge, in particular recognizing that many of the theoretical and experimental approaches that have underpinned the evolution of Si devices with SiO_2 and Si oxynitride dielectrics, and poly-Silicon gate electrodes do not apply for transitional metal oxides and silicates, and ferroelectric and ferromagnetic complex oxides.

This article incorporates a four level approach in which the objective is to develop a science knowledge base that effectively underpins device technology. These four levels are: (i) atomic structure and bonding, including intrinsic bonding defects; (ii) a theoret-

* Corresponding author. Address: North Carolina State University, Department of Physics, Campus Box 8202, Raleigh, NC 27695-8202, USA. Tel.: +1 (919) 515 3938; fax: +1 (919) 515 6538.
E-mail address: lucovsky@ncsu.edu (G. Lucovsky).

0038-1101/$ - see front matter © 2009 Elsevier Ltd. All rights reserved.
doi:10.1016/j.sse.2009.10.012

ical approach for band edge electronic structure, and intrinsic bonding defects consistent with the strongly correlated transition metal d, and rare earth atom f states; (iii) spectroscopic approaches that identify band edge electronic states, and the intrinsic bonding defects; and (iv) intrinsic limitations of device performance and reliability, as determined by the fundamental electronic structure of elemental and complex, as well as intrinsic bonding defects, associated primarily with O-atom vacancies.

This article addresses two issues in which this approach is crucial: (i) intrinsic bonding defects in HfO_2 and TiO_2, focusing on interpretation of spectroscopic data in the context of many-electron theory, and (ii) atomically engineered functionality of complex oxides by controlled introduction of occupied transition metal atom d^n, $n > 1$, states and/or creation of mixed valence bonding by controlled introduction of non-stoichiometric compositions. The thread that connects these two issues is related to the theoretical approach used to interpret spectra associated with occupied d- and f-states, and thereby developing a science knowledge base for understanding limitations imposed by intrinsic bonding defects in transition metal oxide dielectrics, and the opportunities for creative materials engineering targeting increased functionality in complex oxides.

2. Intrinsic defects in HfO_2 and TiO_2

2.1. Experimental and theoretical approach

The TM elemental oxides addressed in this study, TiO_2 and HfO_2, are nano-crystalline thin films, typically 2–6 nm thick. These films have been deposited by remote plasma-assisted CVD onto passivated Si and Ge substrates, and annealed in Ar at 700–900 °C [5–7].

X-ray absorption spectroscopy (XAS) has been used to obtain O K edge spectra at the Stanford Synchrotron Radiation Lightsource on Beam Line 10–1 [6,7]. Spectra were obtained in (i) the pre-edge shake-of regime, <530 eV, below the conduction band edge, (ii) the conduction band regime ~530–545 eV, and (iii) the vacuum continuum shake-off regime, >545 eV, above the conduction band states, or effective ionization potential (IP) of oxygen. Spectra were acquired under conditions which were enabling for obtaining second derivative spectra which are important for identifying Jahn–Teller (J–T) term splittings, as well as defect states features in these pre-edge, and vacuum continuum regimes [5,6]. The number of features in 2nd derivative O K pre-edge and virtual bound state (VBS) regimes that border on the conduction band distinguish between O atom mono- and di-vacancies. When combined with soft-X-ray photoelectron spectroscopy (SXPS), visible-vacuum-ultra-violet spectroscopic ellipsometry (vis–VUV SE) and depth resolved cathodoluminescence spectrosocopy (DRCLS), this approach demonstrates that features in each of these spectra provide a self-consistent many-electron description of the electronic structure that unambiguously distinguishes between mono- and di-vacancy defects.

The transition metal oxides of this section, and the complex oxides of the next fall into a class of strongly correlated many-electron systems in which the strong local repulsion between electrons plays a crucial and determinant role [3,4,8]. This many-electron approach was introduced more than 60 years ago, and applied to the spectra of many-electron atoms [9]. In this application, electronic structure associated with electron transitions in the valence shells was based on spherical symmetry. However when applied to transition metal and rare earth elemental and complex oxides, the symmetry is determined by the nearest-neighbor, or more generally the ligand field [3,4,8] These symmetries play the determinant role in defining the occupation and number of the discrete electronic initial and final states.

The electronic structure of Ti and Hf atoms bordering vacancies is based on an implementation of this symmetrized many-electron theory as applied to occupied d-states of TM atoms [6]. The notation developed below, and the character of the electronic states is directly applicable to describing the electronic states of the Hf or Ti atoms that border on a mono-vacancy (hereafter vacancy) site in CaF_2-structured HfO_2 or rutile structured TiO_2 after removal of a neutral O atom. There are several different oxides of Ti, and TiO, Ti_2O_3 and TiO_2 are used to illustrate the d^n notation. In the ionic model, which is the starting point for applying many-electron theory, the formal valence states for Ti atoms in these oxides are obtained by setting the charge on O-atoms to -2. Neutral atomic states of Ti and Hf are described by s-, p-, and d-shell occupancies: Ti as $4s^23d^2$ and Hf as $6s^25d^2$ [1]. Since s-states have the highest energies with respect to vacuum [10], they are removed first in ion formation. Formal charges on the respective Ti oxide atoms above are Ti^{2+}, Ti^{3+} and Ti^4. TiO is a d^2 oxide and a metal, Ti_2O_3 is a d^1 oxide and a narrow band gap semiconductor, and TiO_2 is a d^0 oxide and an insulator. The ground state electronic configurations for oxides with occupied d-states, d^n, with $n > 1$, explain these very different properties. In each instance the ground state configuration includes the required strongly correlated character. The occupied electron states are above the valence band edge and a are the source of the systematic changes in oxide character noted above [1]. The T_{2g} band in TiO is partially occupied, hence metallic conductivity, and the narrow bandgap of ~0.5 eV in Ti_2O_3 results from a symmetry splitting of the T_{2g} state between a fully-occupied A_1 state and a doubly degenerate E state. d^0 TiO_2 is an wide bandgap semiconductor, $E_g \sim 3$ eV [2].

In these strongly correlated systems, the removal of a neutral O-atom reduces the average ionic charge in TiO_2 and HfO_2 from +4 to +4 – d(N), where N is the fractional concentration of O-atom vacancies. This is better described by creating two populated Ti^{3+} ionic states per removed O. Based on the Pauli exclusion principle, essentially Hund's rule [2], the lowest energy configurations is high spin d^1 state within a T_{2g} manifold of d-states. The formalism for treating intra-atomic d-state transitions in the d^n configurations is well established [11] and will be used as a basis for defining the electronic structure of the intrinsic bonding defects in HfO_2 and TiO_2. A mono-vacancy is represented by two inequivalent and coupled d^1 states, and a di-vacancy by four coupled d^1 states, where the coupling removes the degeneracy of the respective pairs or quartets of ground state electrons so that they are equivalent, respectively, to high spin d^2 and d^4 configurations. The energy separation of this states is established by SXPS studies that indicate two separate and distinct band edge features for both HfO_2 and TiO_2 nano-grain films, essentially the same as those addressed below [5–7,12].

2.2. Spectroscopic data and data reduction

Fig. 1a displays the 2nd derivative pre-edge O K edge XAS spectrum for a 6 nm thick textured nano-grain TiO_2 film of Ge(1 0 0) [13]. This film displays four separate features consistent with a pair of electronically inequivalent d^1 states. These are assigned to d-d′ intra-Ti-atom shake-up transitions associated with a mono-vacancy defect, hereafter simply a vacancy defect [1,3]. Two features per d^1 state are consistent with the doublet character of the crystal field split many-electron theory description.

Spectra for the same 6 nm thick TiO_2 film in VBS shake-off regime reveal four d-d^* transitions corresponding to two pair of doublet virtual states above the ionization are IP limit for each d^1 state; these are displayed in Fig. 1b. Similar pre-edge and VBS regime spectra have also been obtained for TiO_2 2 nm and 4 nm thick films, also grown on Ge substrates. This confirms the textured in-plane growth, and is consistent with the observed d-d′ and d-d^* intra-atom transitions.

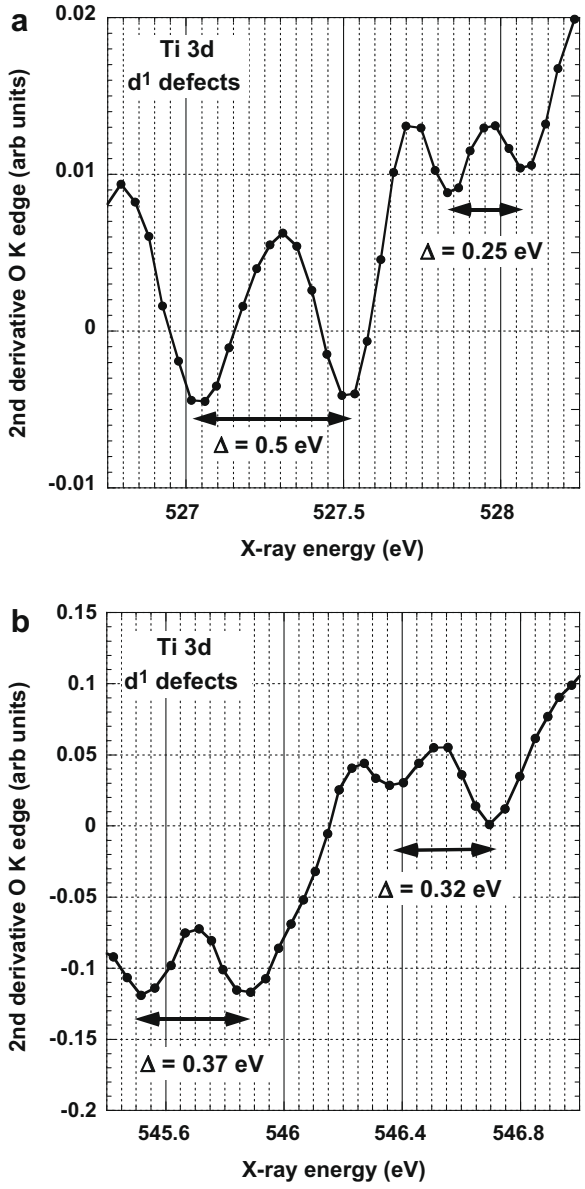

Fig. 1. Second derivative O K edge XAS spectra for a 6 nm thick textured nano-grain TiO_2 film of Ge(1 0 0): (a) pre-edge regime for X-ray energies <530 eV, and (b) virtual bound state regime for X-ray energies >545 eV.

Fig. 2 includes a comparison of the O K spectra of nano-grain monoclinic (m-) HfO_2 and tetragonal (t-) HfO_2 in the spectral regime of the conduction band states. The t-HfO_2 films is grown on a nitrided SiO_x, $x < 2$, interface on Si(1 0 0) and the m-HfO_2 film is grown on Ge(1 0 0). In each instance, films must be more than 3 nm thick to show Jahn–Teller term splittings of Hf d-states [5–7]. These two nano-grain morphologies are readily distinguished by the band edge E_g state structures, two distinct spectroscopic features for the m-HfO_2 nano-grains, but only one for the t-HfO_2 nano-grains. Fig. 3a displays the 2nd derivative pre-edge spectra for the same two films in Fig. 2. Each of these shows the four features assigned here to an inequivalent and coupled pair of d^1 states, characteristic of d-d′ transitions for a vacancy defect. The spectral width of the four features t-HfO_2 is larger compared to the width in m-HfO_2, and is associated with a larger crystal or ligand field splitting. This is consistent with the increased Hf coordination of eight in t-HfO_2, as compared with the coordination of seven in m-HfO_2.

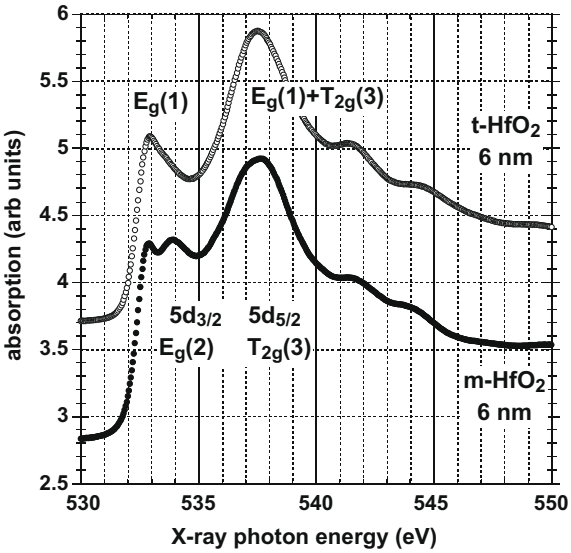

Fig. 2. Comparison of O K spectra for nano-grain monoclinic (m-) HfO_2 and tetragonal (t-) HfO_2 in the conduction band state spectral regime for X-ray energies between 530 and 550 eV.

Fig. 3b displays the corresponding 2nd derivative VBS O K edge spectra, also displaying four features associated with shake-off d-d^* transitions to states above the effective IP for transitions from the O 1s state as defined by the top of the conduction band. Each of the spectral traces for these vacancy defect states is bracketed on the low eV side by the conduction band, and the high energy side of anti-bonding different symmetry f-state features associated with a shallow HFf 4f shake off process as well [14,15]. It is significant to note that the spectral features are at essentially the same energies in both nano-grain materials, while the respective crystal field splittings of the molecular orbital anti-bonding states within the conduction band is different. [6].

2.3. Band edge defects in HfO_2

Conduction band edge traps in HfO_2 have been attributed by the Robertson and Shlugger groups to O-atom monovacancies as distinct from di-vacancies [16,17], and by the energy level diagram from the Pasquarello group as well [18]. Papers by the Lucovsky group initially attributed the spectral features addressed above to di-vacancies [5–7]. This assignment was based on the multiplicity of occupied states at the valence band edge detected by soft X-ray photoelectron spectroscopy (SXPS) [5,6,11], and by assuming that the calculations of Refs. [16–18] which did not indicate band edge defects where characteristic, and correct for mono-vacancy defects. A examination of the similar energy states of neutral and charged O-atom vacancies in Refs. [16–18], in each instance obtained by density functional theory (DFT) methods with modifications targeted to address correlation issues, indicated a significant problem. In each calculation the doubly charged negative vacancy state was a degenerate doublet that is excluded by many-electron theory for strongly correlated oxides. The issue relates on the one hand to fundamental problems with the application of DFT to impurity states in transition metal oxides [19], and by the result of the calculations in which electrons occupying the vacancy states were distributed statistically over the Hf d-states bordering the vacancy. In point of fact it was stated in Ref. [16] that the ground state for the vacancy was a singlet ^1A state. Additionally, these energy level diagrams implied that transitions into these O-atom vacancy states were possible from the top of the valence band, rather than from the occupied d-state levels associated with the vacancy structure.

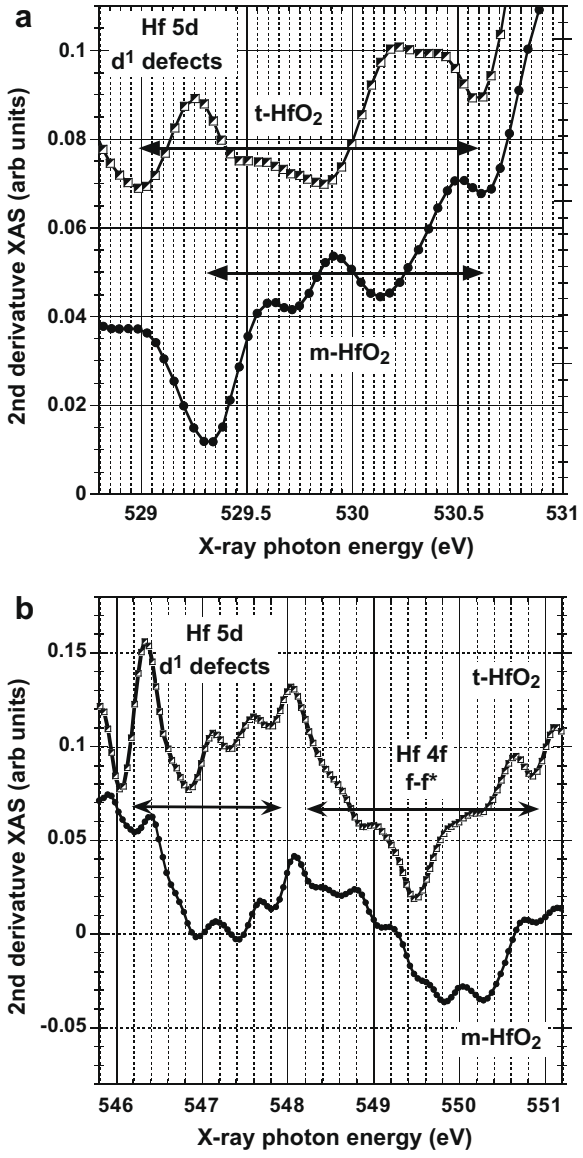

Fig. 3. Second derivative pre-edge spectra for m-HfO_2 and t-HfO_2 films in Fig. 2: (a) pre-edge regime for X-ray energies <530 eV, and (b) Schematic representation of d-state orbitals of (a) virtual bound state regime for X-ray energies >545 eV.

Fig. 4 is energy level diagram for HfO_2 that will be applied to vacancy defects in HfO_2. There is a serious and common misinterpretation of spectroscopic ellipsometry features assigned to defect transitions associated with intrinsic bonding defects, whether they be mono- or di-vacancies. These are intra-impurity state transitions as shown in the panel on the right, rather than transitions from the top of the valence to empty impurity states as suggested in the left-hand panel and obtained by simply inserting the spectroscopic transition energies into an energy band diagram and referencing them to the top of the valence band. The incorrect assignment on the left gave final states in the gap that supported the calculations of the Robertson, Gavartin and Pasquarello groups [16–18], and was assumed to be correct. However, it did not account for the band edge trapping discussed in Ref. [20], and this had to be attributed to a different defect state. However when the transition energies are referenced to the occupied vacancy sites obtained from SXPS, the final states corresponding to the shallow and deep trapping states reported in electrical measurements are obtained [20]. This agreement lends additional support to the energy levels for the coupled pair of d^1 states as proposed in this paper.

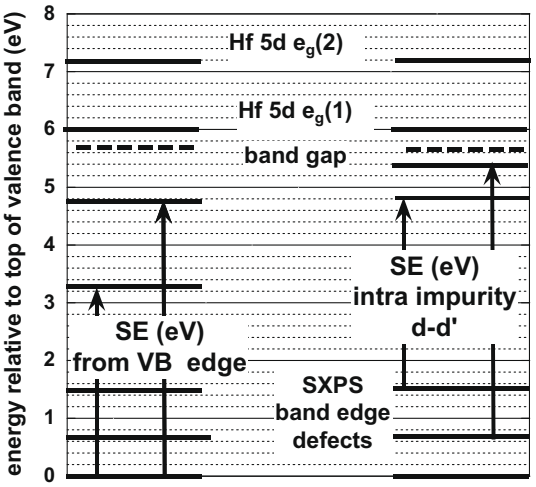

Fig. 4. Initial and final empty states for intra-Hf-atom d-d′ transitions on the right, and on the left, for transitions originating at the top of the valence band.

3. Alloy atoms in complex oxides

3.1. Dopant atom electronic states

The incorporation of a tetravalent dopant or alloy atom such as Ti for trivalent Sc in normally trivalent $GdScO_3$, *forces* Ti into a Ti^{3+} state, producing a d^1 electronic structure [2]. This is a general aspect of substituting a transition metal atom dopant or alloy atoms with a larger number of d-states in their neutral atoms for transition metal (TM) atoms in the complex oxide host. Since both the alloy and host TM atoms must have the same charge state, the substitution for d^0 Sc^3 by d^1 Ti^3 changes the $GdScO_3$ d^0 host to a d^1 complex oxide at the site of the Ti alloy atoms. The Ti for Sc substitution satisfies this condition and this results in a singly occupied Ti 3d d^1 T_{2g} state above the valence band edge. Whereas vacancy defect concentrations in HfO_2 are generally $<10^{19}$ cm^{-3}, there are essentially no limits of Ti solubility in $GdScO_3$ for a composition regime that extends from a doping regime up to 10^{18}–10^{19} cm^{-3}, well into an alloy regime where the properties of the $Gd(Sc,Ti)O_3$ are modified in a significant way. For example, concentrations of Ti in excess of the local volume percolation threshold of 16–17% with respect to Sc, would be expected to lead to an insulator to metal transition with a ferri-magnetic electronic structure, and this is the discussed in sub-sections 3.2 and 3.4. [21].

3.2. Experimental methods: film deposition and X-ray spectroscopy

$Gd(Sc_{1-x}Ti_x)O_3$ alloys >5 nm thick with $x = 0.0$, 0.01, 0.05, 0.18 and 0.25 were deposited at room temperature in an ultra-high vacuum system onto (i) $LaAlO_3$ substrates to promote epitaxial growth, and onto (ii) superficially oxidized Si(0 0 1) to produce nano-grain films. The Ti for Sc substitution results in a Ti^{3+} ionic state, and as such the complex oxide is changed from a d^0 to a d^1 oxide with an occupied Ti T_{2g} state above the valence band edge. Nano-grain dimensions in as-deposited films are <2–2.5 nm, and the coupling between primitive unit cells is too weak to produce Jahn–Teller (J–T) distortions and the subsequent ordering of Ti atoms on the Sc sub-lattice [5,6]. On the other hand, an exchange correlation energy for final states can be estimated from the energy difference between the localized Ti band edge alloy atom state and the first d-state feature of Sc [2]. An insulator to metal transition for the alloy single crystal films grown on $LaAlO_3$ and $SrTiO_3$ (STO) substrates films with $x = 0.18$ and 0.25, a first for intentional doping of a d^0 complex oxide, $GdScO_3$.

The crystal structure in the epitaxial films does not require annealing to promote chemical ordering of the Ti atoms on the Sc sub-lattice sites, and this results in an insulator to metal transition in these as-deposited films for the $x = 0.18$ and 0.25 alloys films. This transition has been confirmed directly by electrical measurements. The same transition has been confirmed by a novel application of X-ray absorption spectroscopy, XAS, using numerical integration of O K edge spectra that extends into the in the pre-edge, and vacuum continuum regimes for X-ray energies <530 eV, and >545 eV, respectively.

3.3. X-ray spectra and data reduction

Fig. 5 displays O K edge spectra for the epitaxial films that introduces a novel way to detect the insulator to metal transition. High levels of charging in the insulating films, $x = 0.0$, $x = 0.01$ and $x = 0.05$ reduce the signal level by more than factor of 30 with respect to substantially higher signal levels with no evidence for charging in the metallic films with $x = 0.18$ and 0.25. The total energy yield, TEY, detection method relies on current flow through the surface of the epitaxial film to balance positive charge associated with photoelectron emission during X-ray irradiation, so that it can easily distinguish between insulating and metallic films.

The significant aspect of the O K edge spectra in Fig. 6 is related to the insulator to metal transition that reveals differences between the energy of the Ti defect/alloy atom state for the 0.25 alloys that are (i) epitaxial films on an STO substrate, and (ii) as-deposited nano-grain films on oxidized Si substrates. The energy difference between the Ti alloy atom states and the lowest energy T_{2g} band edge states is deeper in the gap and shifted to lower energy by ~1 eV with respect to the Ti alloy atom defect in the X-ray amorphous film.

This energy difference is also revealed in the second derivative O K edge spectra in Fig. 7a and b, for two different spectral regimes that include the pre-edge and conduction band energy regimes. These are 528–539 eV in Fig. 7a, and 528–532 eV in Fig. 7b. Consider first the spectra in Fig. 7(a) in the conduction band regime between ~531 eV and 539 eV. These spectra compare the epitaxial films with the nano-grain films in samples that have been annealed

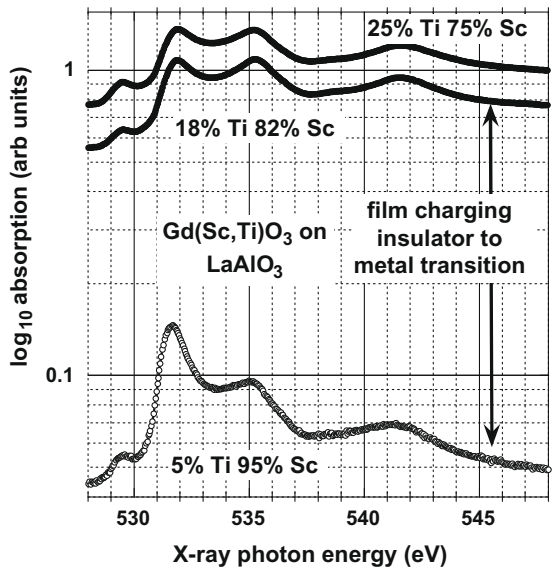

Fig. 5. XAS O K ege spectra of epitaxial $Gd(Sc_{1-x},Ti_x)O_3$ alloys on STO substrates. Films are sufficiently thick so that there are no spectral features due to X-ray absorption in the substrate. Spectra are for films with different Ti concentration: an insulating film with $x = 0.05$ (5%), and two metallic films with $x = 0.18$ (18%) and 0.25 (25%).

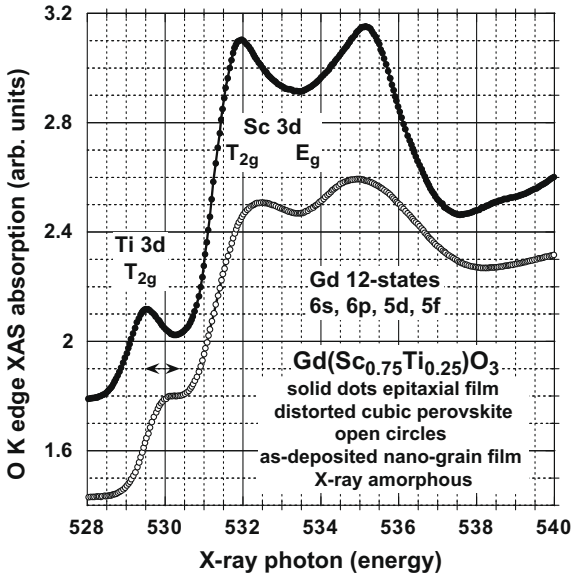

Fig. 6. XAS O K edge spectral for $Gd(Sc_{0.75},Ti_{0.25})O_3$ alloy films. Highlighted are the Ti 3d T_{2g} feature in the pre-edge regime <531 eV, Sc 3d T_{2g} and E_g features centered at ~532 eV, and Gd molecular orbital features centered at ~535 eV. Solid dots are for an epitaxial film, and open dots for abas-deposited X-ray amorphous film on an Si.

to 900 °C. The Gd atoms are in a distorted six fold coordinated site, and the Gd atoms in a 12-fold coordinated and distorted environment as well. The O atoms are six fold coordinated with two different bond lengths for the Sc and Gd neighbors. Grain growth in these annealed nano-grain films is sufficient to reveal the Jan–Teller term splittings in the E_g feature in the nano-grain film [5,6], whereas these splittings are readily evident in the epitaxial films. Specifically, the Sc 3d T_{2g} and E_g, triplet and doublet multiplets are completely resolved in the epitaxial film whereas, the T_{2g} triplet is better resolved in the nano-grain film. These term splitting of the T_{2g} state is consistent with the band edge π-bonding, and E_g doublet splitting with one component of the σ-bonding which also includes Sc 4s and 4p states that overlap the features associated the twelve Gd σ-bonding states, which includes a mix of Gd 6s, 6p, 5d and 5f states. We will not attempt to deconvolve the spectra features between 533 and 539 eV that include a mix of Sc 4s and 4p states and the twelve Gd σ-bonding states as well. Instead the focus will be on the Ti alloy states at the band edge.

Moving onto the second derivative XAS spectra in Fig. 7(b), which display the pre-edge region as well as the Sc T_{2g} states. Consider first the annealed nano-grain spectrum for the alloy with 25% Ti and 75% Sc, and focus on the second derivative minima at ~529.8 eV. The first point is indicated by the lower arrow, labeled "1". This indicates the energy difference, of ~1 eV between the Ti impurity level and the Sc T_{2g} feature that has been already noted in Fig. 6. The value of 1 eV is a final state correlation energy, but from the perspective of the transition energies for excitation of electrons out of occupied states, rather than a spectroscopically determined energy difference between occupied spin states with "up" and "down" character [2]. This energy difference is addressed in Fig. 8, which displays the SXPS spectrum of the epitaxial film.

Returning to Fig. 7b. the upper arrow, labeled "2" indicates the energy difference between the strongly correlated spin band at lower eV, and the weaker opposite spin band in the epitaxial film. This energy difference is also ~1 eV, and the energy difference between the average of this two bands coincides with the position of the center correlation energy defined by the difference in energy between the occupied alloy atom state and the lowest energy T_{2g} Sc d-state. The equality of these two energy differences, each of

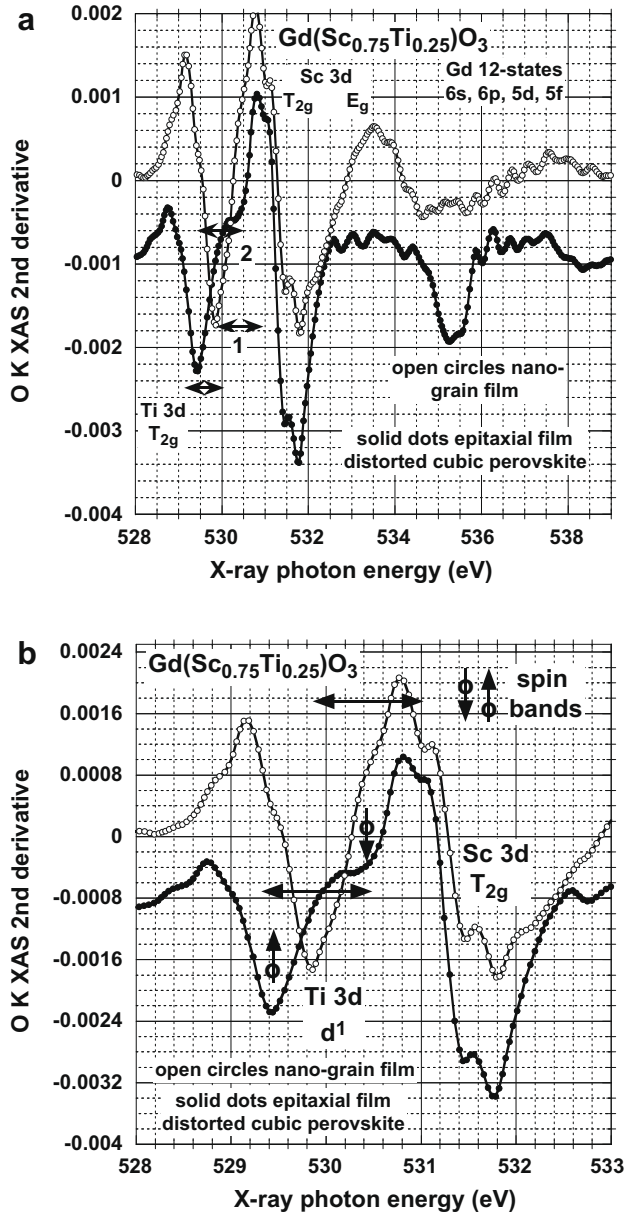

Fig. 7. Second derivative XAS O K edge spectra for the $x = 0.25$, $Gd(Sc_{0.75},Ti_{0.25})O_3$ alloy conduction band and band edge defects states. Arrows 1 and 2 indicate respectively a transition exchange correlation energy: (1) between the energy of the Ti 3d defect state and the lowest Sc 3d T_{2g} state, and (2) between the energy of a correlated majority spin band at ~529.5 eV and the minority spin band at 531 eV: (a) in the spectral range from 528 eV to 539 eV, and (b) from 528 eV to 532 eV.

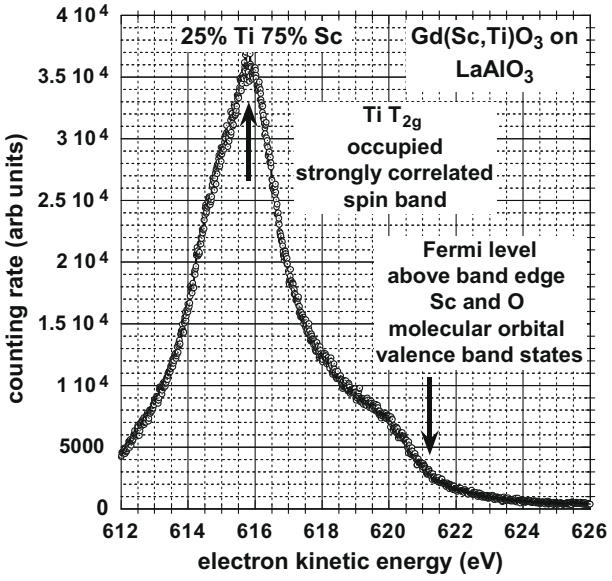

Fig. 8. SXPS valence band spectrum for the $x = 0.25$, $Gd(Sc_{0.75},Ti_{0.25})O_3$ alloy epitaxial film. The occupied Ti_{2g} strongly correlated spin band feature and the Fermi level are marked with arrows.

which is equal to an *effective exchange correlation energy*, is discussed in the next section, and its very existence is an important consequence of the double exchange mechanism for ferro-, or ferri-magnetism which may be present in these films [21].

Another important aspect of the 25% Ti alloy epitaxial film, that is also evident in the 18% Ti alloy film, is the energy difference between the Ti 3d strongly correlated spin state band and the Fermi level. This is indicated in the SXPS spectrum in Fig. 8. The Ti 3d correlated spin band at ~616 eV and is below the Fermi level at ~621 eV, and this is a *characteristic signature* of ferro- or ferri-magnetic behavior in general, and therefore present in metal films, as well as in complex oxides of this article in which there is an insulator to metal transition [2]. This energy difference is about two times the T_{2g}–E_g crystal field (C-F) splitting for TiO_2, and for octahedral complexes in general [2,5,6]. It is important to note that the Fermi level position in the $GdScO_3$ host is determined by the occupied 4f states of Gd, whereas the edge of the valence band is closer to 618 eV.

3.4. The insulator to metal transition

There are two different mechanisms for coupling of electron spins for occupied d^n, $n > 1$ transition metal atoms in TM elemental and complex oxides. The super exchange mechanism prevails in most d^n TM elemental oxides, with $n \geqslant 1$, and is which may be present in these films based on the inherent symmetry of TM dπ – O atom pπ – TM dπ coupling or equivalently, TM dσ – O atom pσ – TM dσ coupling. This produces a d-p-d generic symmetry determined anti-ferromagnetism in the vast majority of first row TM elementals [22]. There are at least two noteworthy exceptions: CrO_2, and the mixed valence oxide Fe_3O_4. A double exchange mechanism prevails in the mixed valence oxide Fe_3O_4. This derives from a homogeneous alloy mixture of FeO and Fe_2O_3 with formally divalent and trivalent Fe, respectively [2]. A similar mechanism also prevails in CrO_2, but the quantitative and qualitative aspects of the magnetic behavior are different [23].

The objective of the research described in this part of the article is to demonstrate that the insulator–metal transition required for the double exchange mechanism could be achieved in an "intelligently-designed" complex oxide and detected spectroscopically as well. The double exchange mechanism is dynamic and based on many-body theory in which the metallic state is a mixture of multiple ionic states with different formal valence [2,21]. The alloy system that we have chosen was anticipated to have an insulator to metal transition when the concentration of Ti^{3+} on the Sc sublattice exceeded a volume percolation threshold of 16% [24]. The means that the occupied Ti d-states in the d^1 configuration experience a substantial degree of connectedness so that a strongly correlated spin up (or spin down) band is generated. This is indeed the case as illustrated in the spectra in Figs. 7 and 8. The magnitude of the exchange correlation energy determines whether ferro- or ferri-magnetic behavior prevails. In this system that energy is ~1 eV, and comparable to width of the occupied strongly correlated spin band, so that ferri-, rather than ferro-magnetism prevails.

Summarizing the results presented in Section 3. Nano-grain and epitaxial thin films of $Gd(Sc_{1-x}Ti_x)O_3$ alloys >5 nm thick with

x = 0.0, 0.01, 0.05, 0.18 and 0.25 have been prepared and studied by XAS and XPES. These studies have identified an insulator to metal transition for films with x = 0.18 and 0.25, consistent with a strongly correlated Ti 3d state metallic conductivity band. Future studies will oxides, and combine XAS, XPES spectroscopic studies with electrical and magnetic measurements as well, and be extended to other alloys in which d^n states with $n > 1$ result.

4. Discussion: strongly correlated transition metal states: intrinsic bonding defect in HfO_2 and Ti d^1 states in $GdSc_{1-x}Ti_xO_3$

As already note, it has been recognized for at least ten years that the ultimate limits of Si device scaling with increased performance and functionality require the replacement of thermally grown and deposited SiO_2 and Si oxynitride alloy gate dielectrics with transition metal oxides and silicates with higher dielectric constants [1]. Higher dielectric constants allow the use of physically thicker films for the required levels of dielectric capacitance while at the same time maintaining tunneling leakage currents that do not degrade device performance. Therefore it is important to understand both experimentally, and theoretically, science base differences between defect and band edge states in SiO_2 and transition metal oxides and silicates. This has been addressed in Section 2, where these differences were demonstrated by a mix of spectroscopic methods, and explained in the context of many-electron theory [2].

In addition to extending the performance of gate dielectrics below an equivalent oxide thickness of 1–1.5 nm, and therefore requiring high-k transition metal dielectrics, there has been also a desire to increase chip functionality, e.g., by introducing ferromagnetic and ferroelectric thin film layers [2], and in particular multiferroic materials in which there are opportunities for novel device configurations with coupled magnetic and ferroelectric functionality [3]. This article has demonstrated in Section 3 that an insulator to metal transition can be introduced into a d^0 complex oxide, $GdScO_3$, by introduction of a normally tetravalent transition metal, Ti, onto trivalent Sc sites, thereby creating a d^1 electron state for each substituted Ti atom.

The spectroscopic studies reported in Sections 2 and 3 have demonstrated the importance of occupied TM atoms in understanding limitations in one case, the electronic structure of vacancy defects in HfO_2, and opportunities in another, the introduction of a insulator to metal transition by alloying into a normally insulating and non-magnetic complex oxide, $GdScO_3$.

The electronic structures associated with the vacancy defects, and the alloy substitution discussed in Sections 2 and 3 could only be explained by using a theory that applies to strongly correlated systems [2,4,8,19], and is different in many important qualitative ways that the theories have addressed SiO_2 gate dielectrics, and the Si–SiO_2 interface. This requires the development of a new paradigm that takes into account differences between this challenge, and in particular recognizing that many of the theoretical and experimental approaches that have underpinned the evolution of Si devices with SiO_2 and Si oxynitride dielectrics, and poly-Silicon gate electrodes do not apply for transitional metal oxides and silicates, and ferroelectric and ferro-magnetic complex oxides.

Note added in proof

This note presents an additional example of how interpretation of spectroscopic data using many-electron theory provides significant insights into the electronic states in complex oxides. Experimental verification of mixed valency has been obtained by comparing O K edge spectra of $LaMnO_3$ and $La_{0.8}Sr_{0.2}MnO_3$. Newly obtained XAS O K edge spectra have indicated changes characteristic of an insulator to metal transition for the 20% Sr for La atom substitution, as well as mixed valency. These include (i) a change from a distorted perovskite structure in $LaMnO_3$ to a cubic perovskite in $La_{0.8}Sr_{0.2}MnO_3$, (ii) pre-edge shake-up, and vacuum continuum shake-off features consistent with the d^4 character of Mn^{3+} in $LaMnO_3$, and (iii) additional sharp features in the shake-up and shake-off regimes in $La_{0.8}Sr_{0.2}MnO_3$ consistent with the d^3 character of the Mn^{4+}. Additionally, These spectral changes confirm that E_g symmetry electron of the d^4 configuration contributes to the metallic conductivity consistent with a schematic representation of double exchange by Cox in Ref. [2]. The mixed valency is also confirmed by the multiplicity and relative energies of features in the $MnL_{2,3}$ specturm.

$La_{0.8}Sr_{0.2}MnO_3$ alloy and Fe_3O_4 are examples for the double exchange mechanism applied to $La_{1-x}Ca_xMnO_3$ by De Gennes [21] and proposed originally by Zener [22]. This mechanism predicts the relative ease of electron *exchange* between two transition metal d^n, n>1 ion states, each with different values of n, such as Mn^{3+} d^4 and Mn^{4+} d^3 in $La_{0.8}Sr_{0.2}MnO_3$. The mechanism relies on electron transport in which the *exchanged* electron does not change spin, preserving the Hund's rule occupancy that is crucial for ferromagnetism. This leads to ferromagnetic alignment in $La_{0.8}Sr_{0.2}MnO_3$, where metallic behavior results from the Sr concentration of 20% exceeding a percolation threshold, ~17% [23].

Whereas double exchange mechanism relies on mixed valency to promote ferromagnetic behavior, not all mixed valence materials display double exchange and/or ferromagnetism [24,25]. Ferromagnetism in $La_{1-x}Ca_xMnO_3$ alloys, which are isolectronic analogs of $La_{1-x}Sr_xMnO_3$, is dependent on both composition, x, and temperature, demonstrating that additional factors are important for this cooperative behavior.

There is no spectroscopic evidence for mixed valency in $GdSc_{0.75}Ti_{0.25}O_3$ alloy of this article. This has been established by recently obtained $L_{2,3}$ spectra which confirm the d^1 configuration for substituted Ti^{3+}, and the d^0 configuration for host Sc^{3+}. It unlikely that a double exchange process would derive from a mixing of the Ti d^1 state with occupied Gd f^7 states.

References

[1] Houssa M, Hyens MM. in: Houssa M, editor, High-k gate dielectrics. Bristol: Institute of Physics; 2004 [Chapter 1.1].
[2] Cox PA, Transition metal oxides. Oxford: Clarendon; 1992 [chapters 2, 3 and 5].
[3] Cheong S-W, Mostovoy M. Nat Mater 2007;6:13.
[4] Cotton FA. Chemical applications of group theory. 2nd ed. New York: Wiley Interscience; 1963 [chapter 8].
[5] Lucovsky G, Seo H, Lee S, et al. Japan J Appl Phys 2007;46:1899.
[6] Lucovsky G. J Mol Struct 2007;838:187.
[7] Lucovsky G et al. Microelectron Eng 2009;86:1676.
[8] de Grott F, Kotani A. Core level spectroscopy of solids. Boca Ratan: CRC Press; 2008 [chapter 4].
[9] Condon EU, Shortley GH. The theory of atomic spectra. London: Cambridge University Press; 1957 [chapters VI–X].
[10] Harrison WA. Elementary electronic structure. Singapore: World Scientific; 1999.
[11] Koiller B, Falicov LM. J Phys C: Solid State Phys 1974;7:299.
[12] Fleming L et al. J Appl Phys 2007;120:033707.
[13] Lucovsky G et al. Microelectron Eng 2007;84:2350.
[14] Teo BK. EXAFS: basic principles and data analysis. Berlin: Springer Verlag; 1986 [chapter 5].
[15] Stöhr J. NEXAFS spectroscopy. Berlin: Springer; 2003 [chapters 2 and 4].
[16] Xiong K, Robertson J, et al. Appl Phys Lett 2005;87:183505 [and reference therein].
[17] Gavartin JL, Ramo DM, et al. Appl Phys Lett 2006;89:082908 [and reference therein].
[18] Broqvista P, Pasquarello A. Appl Phys Lett 2006;89:262904.
[19] Bersuker IB. J. Comput Chem 1997;18:260.
[20] Autran JL, et al. In: Houssa M, editor, High-k gate dielectrics. Bristol: Institute of Physics; 2004 [chapter 3.4].
[21] DeGennes PG. Phys Rev 1960;118:141.
[22] White RM, Geballe TH. Long range order in solids, solid state physics supplement 15. New York: Academic Press; 1979 [chapter IV].
[23] Scher H, Zallen R. J Chem Phys 1970;53:3759.
[24] Korotin MA, Anisimov VI, Khomskii DI, et al. Phys Rev Lett 1998;80:4305.
[25] Varma CM. Rev Modern Phys 1976;42:219.